# Elucidating the Behavior of the SARS-CoV-2 Virus Surface at Vapor-Liquid Interfaces using Molecular Dynamics Simulation

**Florian Fleckenstein**[a], **Simon Stephan**[a,1], **and Hans Hasse**[a]

This manuscript was compiled on January 26, 2024

**Aerosols play a major role in the transmission of the SARS-CoV-2 virus. The behavior of the virus within aerosols is therefore of fundamental importance. On the surface of a SARS-CoV-2 virus, there are about 40 spike proteins, which each have a length of about 20 nm. They are glycosylated trimers, which are highly flexible, due to their structure. These spike proteins play a central role in the intrusion of the virus into human host cells and are, therefore, a focus of vaccine development. In this work, we have studied the behavior of spike proteins of the SARS-CoV-2 virus in the presence of a vapor-liquid interface by molecular dynamics (MD) simulations. Systematically, the behavior of the spike protein at different distances to a vapor-liquid interface were studied. The results reveal that the spike protein of the SARS-CoV-2 virus is repelled from the vapor-liquid interface and has a strong affinity to stay inside the bulk liquid phase. Therefore, the spike protein bends when a vapor-liquid interfaces approaches the top of the protein. This has important consequences for understanding the behavior of the virus during the dry-out of aerosol droplets.**

SARS-CoV-2 | Molecular Dynamics | Vapor-Liquid Interface | Airborne Transmission

## Significance Statement

In this work, the behavior of the SARS-CoV-2 virus at vapor-liquid interfaces is investigated. This is crucial for understanding the transmission route in aerosole droplets since the virus is airborne. The research question addressed here is, whether the virus particle has a preferential residency at droplet surfaces or in a liquid bulk phase. No information on this important question is presently available in the literature. Therefore, we carried out molecular dynamics simulations of the virus surface and its interaction with a vapor-liquid interface. The results clearly show that the SARS-CoV-2 virus has a preferential residency in the liquid bulk phase. This has important implications for the structure and biological functionality of the virus surface, i.e. its infectiousness, during aerosol evaporation.

The SARS-CoV-2 virus is often found in aqueous solutions and its structure in water has been studied both by molecular simulations and experimental techniques (1–5). However, there are many situations in which the virus in water comes into contact with a vapor-liquid interface, e.g. during the transmission in aerosols, inside the respiratory tract or the gastrointestinal tract, as well as on surfaces contaminated with aqueous solutions containing SARS-CoV-2. However, the interactions of the SARS-CoV-2 virus with vapor-liquid interfaces are presently unknown. The key question here is: is the virus attracted or repelled by the interface, as this has important consequences for all situations mentioned above: it makes a difference, whether the viruses are found mainly on the surface or in the bulk water.

**Approach.** Studying the behavior of SARS-CoV-2 at vapor-liquid surfaces is challenging. Suitable experimental techniques do not exist, so that we must rely on simulations. To have a chance to be predictive, molecular simulations based on suitable atomistic force fields must be used; which, however, imposes strong restrictions on the size of the object that can be studied. We have tackled this here by studying only the (glycosylated) S protein, embedded at its stalk in a section of the virus membrane, and immersed in water with a vapor-liquid interface. The second issue is time. Even the spatially restricted scenario contains millions of interactions sites. Its behavior can only be studied for times in the nanosecond range, which can be insufficient to obtain full equilibration. This was tackled here by carefully choosing the initial conditions and the scenario as well as by long simulation times. The response of the system to changing the distance between the vapor-liquid interface and the spike protein was studied in a series of simulations. The response of the system was so clear, that we trust that the behavior of the macroscopic system can be inferred from the results.

**SARS-CoV-2 Virus.** The SARS-CoV-2 virus has a diameter in the range of 50 to 150 nm (without spike proteins) and the spike (S) proteins have a length of about 20 nm (4). On average, 40 S proteins reside on the lipid bilayer membrane of the virus (4). This leads to an average distance between the S proteins on the membrane, which is of the same order as the spike length. The S proteins are themselves densely covered in a glycan coat for protection against immune system antibodies (1, 2, 6). The structure of the S protein can be divided into a head region, a stalk region, a

Author affiliations: [a]Laboratory of Engineering Thermodynamics (LTD), RPTU Kaiserslautern, Erwin-Schrödinger-Straße 44, 67663 Kaiserslautern, Germany

FIFI: Data Curation, Formal analysis, Writing - Original Draft; SiSt: funding acquisition, Conceptualization, Methodology, Supervision, Writing - Review & Editing; HaHa: funding acquisition, Conceptualization, Writing - Review & Editing.

There are no conflicts of interest to declare.

[1]To whom correspondence should be addressed. E-mail: simon.stephanrptu.de

trans-membrane region, and a cytoplasmic tail. Turoňová et al. investigated the flexibility of the S protein by experiment and molecular simulation, revealing further subdivisions of the S protein stalk region into an upper and lower "leg" along flexible hinges, namely "hip", "knee", and "ankle" (4), which make the SARS-CoV-2 S proteins particularly flexible. The three receptor binding domains (RBDs) of the S protein head have conformational variability. In its closed conformation, the three RBDs are in a "down" configuration, whereas in its open conformation, one RBD is in an "up" configuration (extending outwards). This reduces the coverage of the glycan coat (2). Both conformations were found to be populated approximately 50:50 at ambient conditions (4). S proteins are used by the virus to enter the host cell (5, 7).

**Aerosols.** Airborne transmission via aerosols is the main transmission route of the SARS-CoV-2 virus (8, 9). Aerosols (droplets smaller 5 $\mu$m) can remain in the ambience for several hours (8). The vapor-liquid interface of aerosol droplets is a dominant feature, as the droplets have a relatively high surface-to-volume ratio and decrease in size during droplet dry-out (8). Hence, the behavior of the SARS-CoV-2 virus at vapor-liquid interfaces, i.e. affinity to the interface, is important for understanding the transmission route of the virus and during the dry-out of aerosol droplets. In the aerosol droplet, the virus can, in general, reside either in the liquid bulk or at the vapor-liquid interface. The preferential residency is presently unknown. Similar arguments apply to other situations, in which the SARS-CoV-2 virus in water comes into contact with vapor-liquid interfaces.

**All-Atom MD Simulations.** To elucidate the behavior of the SARS-CoV-2 virus at vapor-liquid interfaces, molecular dynamics (MD) simulations of a representative part of the virus surface were carried out comprising the lipid bilayer membrane and a S protein. Large-scale all-atom MD simulations were performed for both the closed (PDB ID: 6VXX)(5) and the open conformation (PDB ID: 6VSB)(1). In the closed conformation, the three RBDs are in the "down" conformation, whereas in the open conformation one of the RBDs is in the "up" configuration. For the simulations, fully-glycosylated S protein structures were taken from literature (2) and were then embedded (10) in a membrane model taken from Ref. (2). For both S protein conformations (closed and open), a simulation set-up was prepared in subsequent steps and studied, in which a representative part of the virus surface is present in the vicinity of a vapor-liquid interface. Initially, the distance between the membrane and vapor-liquid interface is roughly 40 nm. Further details are given in the Supporting Information.

For both conformations, the influence of the distance of the vapor-liquid interface and the S protein on the conformation of the system was studied in a series of simulations in which in each step about 0.6% of the water molecules from above the bilayer were removed. This can be considered as representing an open evaporation process. The removed water molecules were randomly selected from the bulk water (distance of at least 1.2 nm to the S protein). The removed amount of water molecules is represented as $\Phi = N^{\mathrm{r}}_{\mathrm{H_2O}}/N^{0}_{\mathrm{H_2O}}$ in the following, in which the superscript indicates the removed (r) or initial (0) amount of water molecules above the bilayer. Each removal step was followed by a 0.5 ns re-equilibration and 0.5 ns production run, in which properties of the S protein were sampled. The distances and angles characterizing the configurational changes were sampled. Hence, the evaporation process was modeled in a somewhat simplyfied way, which might in general influence the results. Yet, the interaction of the overall virus surface with the vapor-liqiud interface is not expected to be affected by that.

The simulations were carried using the open source code GROMACS (11) Version 2022. The force field models were adopted from the CHARMM-GUI (10) and MolMod (12) program. The CHARMM36m force field (13–15) in conjunction with the TIP3P water model (16) and *Beglov and Roux* force fields (17) for the ions was used. The lipid force field parameters were adopted from *Klauda et al.* (18).

## Results

Figure 1 shows simulation snapshots of four states during the emulated evaporation process for the open conformation. The corresponding results for the closed conformation, which are similar, are presented in the Supporting Information. In the initial state (Fig. 1A) in which the distance between the top of the S protein and the vapor-liquid interface is about 13 nm, there is no significant bending of the S protein. The RBD (highlighted in transparent red) is oriented outwards. As the vapor-liquid interface approaches the virus (Fig. 1 B to D), the S protein bends significantly in its stalk region. This clearly indicates that the SARS-CoV-2 S protein has a strong affinity to stay inside the liquid bulk phase. In the last state (Fig. 1D), the SARS-CoV-2 S protein lies basically flat on the membrane, and in doing so even deforms the membrane, to stay inside the liquid bulk phase.

For quantifying the structural changes of the S protein, different observables were sampled. Results are shown in Figure 2A for the distance between the vapor-liquid interface and the closest atom of the S protein ($z_1$), the interface and the center of mass (COM) of the RBD in the "up" position ($z_2$), the interface and the COM of the S protein head ($z_3$), and the interface and the membrane ($z_4$) (Fig. 2B). Figure 2 shows that the distances $z_1$ to $z_4$ change significantly throughout the evaporation process. Until $\Phi \approx 30\%$, all four distances decrease approximately linearly and with a similar slope. In this phase, the SARS-CoV-2 S protein shows little deflection as the vapor-liquid interface approaches. This behavior changes, as the distance $z_1$ becomes smaller than 5 nm. Then, in the second phase, the distance between the S protein and the interface stays roughly the same during the dry-out, indicating that the S protein deflects. This phase ends at $\Phi \approx 55\%$ when the S protein lies essentially flat on the membrane, so that it cannot move further away from the vapor-liquid interface. Upon further removal of water, in the third phase again a linear decrease in all four distances is found. The series of simulations ends when the vapor-liquid interface reaches the top of the S protein (Fig. 1D).

The S protein of the SARS-CoV-2 virus exhibits a high flexibility in the stalk region, as highlighted by Turoňová et al. (4). Our results indicate that this stalk flexibility is important when a virus particle approaches a vapor-liquid interface. In this work, a deflection angle $\delta$ is defined as the deflection of the section between the center of mass (COM) of the S protein and the transmembrane region normal to the interface, i.e. a deflection of 0° corresponds to no deflection. The results for

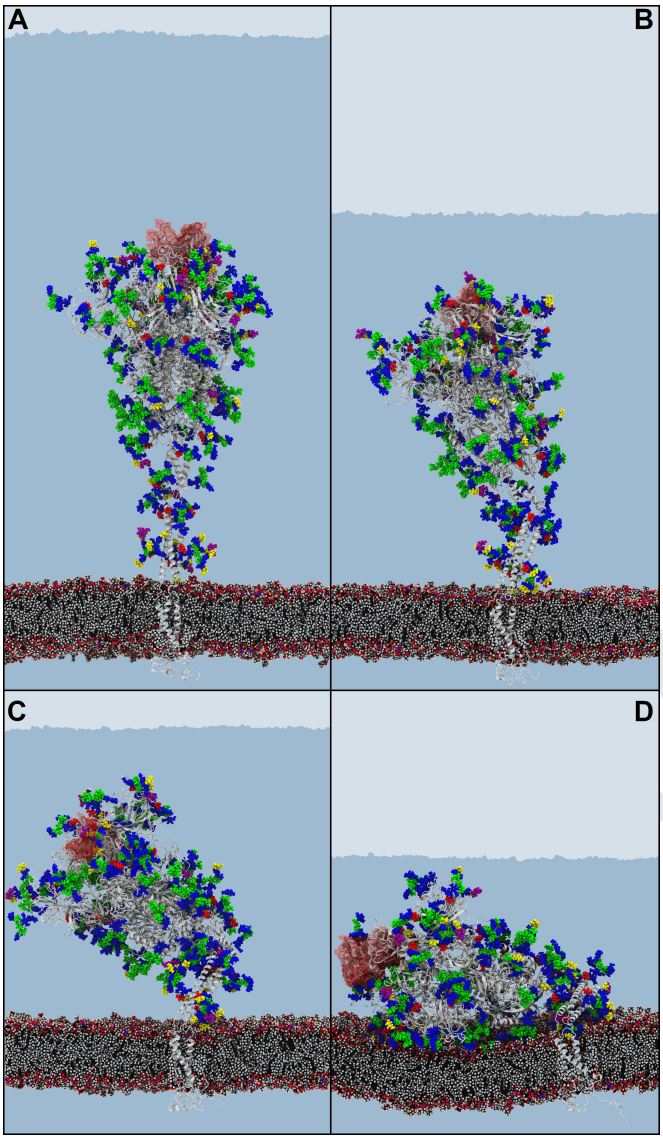


**Fig. 1. Visualization of the evaporation process for the open conformation all-atom simulations.** (A) initial configurations, i.e. no water molecules removed yet ($\Phi = 0$). (B) $\Phi \approx 30\%$ of water molecules removed. (C) $\Phi \approx 50\%$ of water molecules removed. (D) $\Phi \approx 70\%$ of water molecules removed. The protein is depicted in white. Color code of glycans on the surface of the protein: GlcNAc (blue), mannose (green), fucose (red), galactose (yellow), and sialic acid (purple). Color code of lipid bilayer: C-atoms (black), H-atoms (white), O-Atoms (red), N-Atoms (orange) and P-Atoms (blue). The vapor-liquid interface is indicated as the transition between the differently shaded blues. The outward-facing RBD is highlighted in transparent red.

the deflection angle are shown in Figure 3. Initially, there is little to no deflection which then increases throughout the evaporation process as the vapor-liquid interface approaches the top of the S protein, until it lies flatly on the membrane. The simulation results for the closed conformation, which are presented in the Supporting Information, are similar to those for the open conformation. The simulation results for both the open and the closed conformation are also visualized in movies, which are provided with the Supporting Information (movies S1 and S2).

## Discussion

This work gives insights into the structural behavior of the SARS-CoV-2 S protein near vapor-liquid interfaces. The results indicate that the S protein strongly deflects as the vapor-liquid interface approaches the virus – for both the open and the closed conformation. Hence, the SARS-CoV-2 S protein has a strong preference to stay inside the liquid bulk phase. The flexibility of the S protein is highly important for the conformation of the virus near vapor-liquid interfaces. For small distances, the S protein lies flat on the membrane surface. This might also have important consequences for the structure and biological functionality of the virus surface, i.e. its infectiousness. In future work, it would be interesting to carry out replica simulations and to invert the sequence of the simulations (i.e. to fill up water) to see whether similar results are obtained. It would also be interesting to study the influence of the force field on the results and to investigate neighboring effects by including more than one S protein in the scenario. Last not least, the approach developed here could be applied to other important viruses.

## Materials and Methods

**Investigated Systems.** The SARS-CoV-2 S proteins are homotrimeric class 1 virus fusion proteins, which consist of 1273 amino acid chains per monomer (19–21). They consist of several specific topological regions: an extracellular *N*-terminus, a transmembrane domain anchored in the viral membrane, and a short intracellular cytoplasmic tail (CT) (20). The extracellular part of the S protein can further be divided into a head region and a stalk region, which comprises a lower leg part and an upper leg part. Both regions are shielded by a glycan coat (2). Two conformations of the fully-glycosylated SARS-CoV-2 S protein were studied in this work. The atomistic configurations were taken from the literature (2), which are based on the open (1) and closed (5) state of the spike (S) protein regarding the receptor binding domain (RBD) conformation. The closed conformation S protein structure is based on data determined from cryo-electron microscopy (cryo-EM) resolved at 0.28 nm resolution (PDB ID: 6VXX) (5), for which the RBD's are in the "down" configuration. The open conformation of the S protein structure is based on data determined from cryo-EM microscopy resolved at 0.346 nm resolution (PDB ID: 6VSB) (1), in which one RBD is in the "up" configuration. The SARS-CoV-2 S protein structure studied here comprises both *N*-glycans and *O*-glycans on the protein surface. 22 *N*-glycosylation sites (6) and 2 *O*-glycosylation sites (22) per monomer were used for the SARS-CoV-2 S protein, which are distributed over the proteins surface. The glycosylation population used in this work is based on the site-specific glycoprofile data reported by *Casalino et al.* (2)). In total, 77 glycosylation sites were used – for both the open and closed conformation. These glycans comprise of linear and branched oligo-mannose (in graphical representations *N*-Acetylglucosamine (GlcNAc) is displayed in blue and mannose in green), that were further modified by e.g. fucosylation and sialyation (fucose is displayed in red, galactose in yellow, and sialic acid in purple) (2).

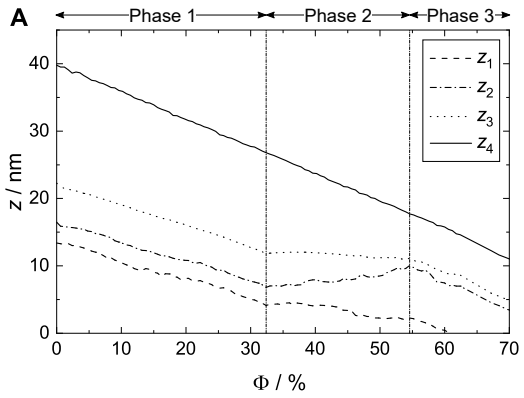


**Fig. 2. Change in observable lengths ($z_1$-$z_4$) during the evaporation process.** (A) Results for open conformation. Changes are presented as a function of the removed amount of water molecules Φ. (B) Definition of observable lengths: interface to the closest atom of the S protein ($z_1$); interface to the COM of the RBD in the "up" position ($z_2$); interface to the COM of the S protein head ($z_3$); and interface to the membrane ($z_4$).

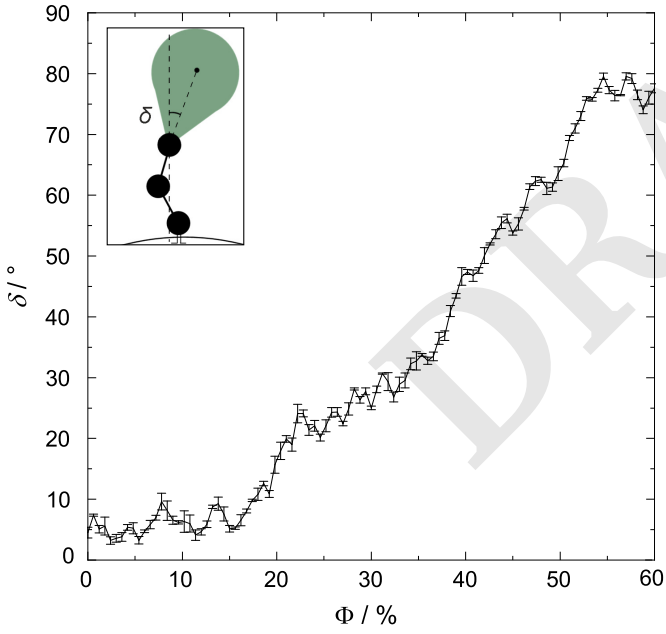


**Fig. 3. Structural changes of the SARS-CoV-2 S protein in the stalk region.** Change of the deflection angle $\delta$ over the course of the process. Changes are presented as a function the removed amount of water molecules Φ. Results for the open conformation.

Of the two potential *O*-glycosylation sites, only one is populated in each of the three monomers (O323). For the first monomer, also the second *O*-glycosylation site (O325) is populated (2). For the modeling of the glycans in the molecular simulations, the force field proposed by *Guvench et al.* (15) was used, which also comprises their glycosidic linkages to the S protein. The lipid composition of the membrane, in which the S protein is embedded, was chosen to mimic the lipid composition of a virus membrane (23, 24). The lipid composition of the membrane was adopted from *Casalino et al.* (2) and the membrane was generated inside of CHARMM-GUI's *input generator* (10, 25, 26). Details are given in the Supporting Information.

**Simulation Scenario Set-up.** To create the simulation scenario for both the open and closed conformation, which is used to analyze the behavior of the SARS-CoV-2 S protein in the vicinity of a vapor-liquid interface, two independent systems (one containing the embedded S protein and the other a vapor-liquid equilibrium of water) were generated that were then combined and re-equilibrated. The total size of the open conformation system was 24.88 nm x 24.88 nm x 95.93 nm and contains 3,434,421 sites. The total size of the closed conformation system is 24.98 nm x 24.98 nm x 95.93 nm and contains 3,681,882 sites. Further details on the generation are given in the Supporting Information. The simulations were carried out at a temperature of $T = 300$ K and an initial concentration of sodium and chloride ions of 150 mM. The leap-frog algorithm was used for the integration of Newton's equations of motion. All simulations were performed using periodic boundary conditions and particle-mesh Ewald (27) electrostatics for long-range electrostatic interactions with maximum grid spacing of 0.2 nm. Short-ranged electrostatic interactions and non-bonded van der Waals interactions were calculated applying a cut-off radius of 1.2 nm. For the van der Waals interactions, a switch function was used to smoothly transition to 0 between the switching distance of 1 nm and the cut-off (28). To allow for a 2 fs integration timestep (or 1 fs during the equilibration of the systems – see the Supporting Information), all hydrogen-containing bonds were constrained by the LINCS algorithm (29).

**Simulation Procedure for the Production Phase Modeling the Evaporation Process.** The simulations were conducted on the ELWE supercomputer at the Regional University Computing Center Kaiserslautern (RHRK) on Intel Xeon Gold 6126 CPU's. The intel compiler (version 2022) along with the intel openMPI version 4.1 (2022) and the GNU (version 11.2.0) compiler was used throughout. All simulations were conducted in parallel using 8 nodes à 24 cores, achieving approximately 3-5 ns per day for the production phase simulations. During the simulations, the position of the vapor-liquid interface with respect to the virus surface was decreased by removing water molecules. This was done step-wise, i.e. some particles were removed at a given time. Then, the system was re-equilibrated, and properties were sampled in a production phase; then, more particles were removed and the process started over such that the evaporation was conducted step-wise. Therefore, 5,000 water molecules were randomly selected and removed from above the lipid bilayer (corresponds to approximately 0.6% of all water molecules above the lipid bilayer initially in the system),

that were at least 1.2 nm away from both protein and lipid bilayer interaction sites. The obtained set-up was then re-equilibrated for 250,000 steps and then a production run of 250,000 steps was conducted. Both, the re-equilibration and the production phase simulations were carried out in the $NVT$ ensemble – with a reduction in $N$ in between each production phase step. During the production phase, structural properties of the S protein and structural properties for characterizing the configuration of the S protein with respect to the vapor-liquid interface were sampled. To continue the evaporation process, this process was repeated to further decrease the distance between the lipid bilayer and the vapor-liquid interface. To study the flexibility of the SARS-CoV-2 S protein, the positions of the CT (amino acids 1235-1273), ankle (amino acids 1211-1213), knee (amino acids 1161-1163), hip (amino acids 1136-1138), and S protein head (amino acids 13-1135) were defined as the center of mass (COM) of the corresponding amino acids and sampled throughout.

**Sampled Properties.** The deflection of the SARS-CoV-2 S protein during the evaporation process was quantified using several characteristic distances. For determining the observable lengths, specific coordinates were determined in the post-processing such as: the position of the vapor-liquid interface, the "outwards" facing side of the lipid bilayer in the $z$ coordinate, as well as the COM of the S protein head and the RBD that is in the "up" configuration of the open system. The $z$-position of the vapor-liquid interface was determined from density profiles during the production phases. The density profiles were sampled as an average of 250,000 timesteps during the production phase for $N = 960$ bins, each with a width of $\Delta z \approx 0.1$ nm. The interface position was defined here as the $z$-position were the local number density was half the difference of the two bulk phases. To compare the structural behavior of the SARS-CoV-2 S protein in both conformations during the evaporation process, additionally the fluctuations of the RBD's in regards to central axis of the S protein were investigated. Therefore, also the COM positions of all three RBD's were sampled. To investigate the flexibility of the stalk region of the SARS-CoV-2 S protein, the angle between the lower leg and the transmembrane domain (defined in this work as $\alpha$ (ankle)), the angle between the upper and lower legs (defined as $\beta$ (knee)), and the angle between the S head COM and the upper leg (defined as $\gamma$ (hip)) were sampled (see the Supporting Information). The angles were specified as the angle between three points in space, i.e. for a perfectly straight stalk region the values for the angles are 180° each. Error estimates were computed block averaging (consisting of 0.167 ns each block) during the production phase.

**ACKNOWLEDGMENTS.** The simulations were carried out on the Regional University Computing Center Kaiserslautern (RHRK) under the grant RPTU-MTD and on NHS machine in Mainz.

The authors gratefully acknowledge funding of the present work by the Deutsche Forschungsgemeinschaft (DFG) under the grant STE 3094/1-1 and HA 1993/22-1.

All data needed to evaluate the conclusions presented in the paper are given in the paper or the Supporting Information, which include further details on the results obtained in this work as well as videos of the reaction of the S protein to the approaching interface.



1. D Wrapp, et al., Cryo-EM structure of the 2019-nCoV spike in the prefusion conformation. *Science* **367**, 1260–1263 (2020).
2. L Casalino, et al., Beyond Shielding: The Roles of Glycans in the SARS-CoV-2 Spike Protein. *ACS Cent. Sci.* **6**, 1722–1734 (2020).
3. Z Ke, et al., Structures and distributions of SARS-CoV-2 spike proteins on intact virions. *Nature* **588**, 498–502 (2020).
4. B Turoňová, et al., In situ structural analysis of SARS-CoV-2 spike reveals flexibility mediated by three hinges. *Science* **370**, 203–208 (2020).
5. AC Walls, et al., Structure, Function, and Antigenicity of the SARS-CoV-2 Spike Glycoprotein. *Cell* **181**, 281–292.e6 (2020).
6. Y Watanabe, JD Allen, D Wrapp, JS McLellan, M Crispin, Site-specific glycan analysis of the SARS-CoV-2 spike. *Science* **369**, 330–333 (2020).
7. CAM de Haan, PJM Rottier, Molecular interactions in the assembly of coronaviruses. *Adv. Virus Res.* **64**, 165–230 (2005).
8. YY Zuo, WE Uspal, T Wei, Airborne Transmission of COVID-19: Aerosol Dispersion, Lung Deposition, and Virus-Receptor Interactions. *ACS Nano* **14**, 16502–16524 (2020).
9. KA Prather, et al., Airborne transmission of SARS-CoV-2. *Science* **370**, 303–304 (2020).
10. S Jo, T Kim, VG Iyer, W Im, CHARMM-GUI: a web-based graphical user interface for CHARMM. *J. Comput. Chem.* **29**, 1859–1865 (2008).
11. MJ Abraham, et al., GROMACS: High performance molecular simulations through multi-level parallelism from laptops to supercomputers. *SoftwareX* **1-2**, 19–25 (2015).
12. S Stephan, M Horsch, J Vrabec, H Hasse, MolMod - an open access database of force fields for molecular simulations of fluids. *Mol. Simul.* **45**, 806–814 (2019).
13. J Huang, et al., CHARMM36m: an improved force field for folded and intrinsically disordered proteins. *Nat. Methods* **14**, 71–73 (2017).
14. J Huang, AD MacKerell Jr, CHARMM36 all-atom additive protein force field: Validation based on comparison to NMR data. *J. Comput. Chem.* **34**, 2135–2145 (2013).
15. O Guvench, E Hatcher, RM Venable, RW Pastor, ADJ MacKerell, CHARMM Additive All-Atom Force Field for Glycosidic Linkages between Hexopyranoses. *J. Chem. Theory Comput.* **5**, 2353–2370 (2009).
16. WL Jorgensen, J Chandrasekhar, JD Madura, RW Impey, ML Klein, Comparison of simple potential functions for simulating liquid water. *The J. Chem. Phys.* **79**, 926–935 (1983).
17. D Beglov, B Roux, Finite representation of an infinite bulk system: Solvent boundary potential for computer simulations. *The J. Chem. Phys.* **100**, 9050–9063 (1994).
18. JB Klauda, et al., Update of the charmm all-atom additive force field for lipids: Validation on six lipid types. *The J. Phys. Chem. B* **114**, 7830–7843 (2010).
19. SC Harrison, Viral membrane fusion. *Virology* **479-480**, 498–507 (2015).
20. BJ Bosch, R van der Zee, CAM de Haan, PJM Rottier, The coronavirus spike protein is a class i virus fusion protein: Structural and functional characterization of the fusion core complex. *J. Virol.* **77**, 8801–8811 (2003).
21. Y Huang, C Yang, Xf Xu, W Xu, Sw Liu, Structural and functional properties of sars-cov-2 spike protein: potential antivirus drug development for covid-19. *Acta Pharmacol. Sinica* **41**, 1141–1149 (2020).
22. A Shajahan, NT Supekar, AS Gleinich, P Azadi, Deducing the N- and O-glycosylation profile of the spike protein of novel coronavirus SARS-CoV-2. *Glycobiology* **30**, 981–988 (2020).
23. J Klumperman, et al., Coronavirus M proteins accumulate in the Golgi complex beyond the site of virion budding. *J. Virol.* **68**, 6523–6534 (1994).
24. J Krijnse-Locker, M Ericsson, P Rottier, G Griffiths, Characterization of the budding compartment of mouse hepatitis virus: evidence that transport from the RER to the Golgi complex requires only one vesicular transport step. *J. Cell Biol.* **124**, 55–70 (1994).
25. EL Wu, et al., Charmm-gui membrane builder toward realistic biological membrane simulations. *J. Comput. Chem.* **35**, 1997–2004 (2014).
26. S Jo, KC Song, H Desaire, AD MacKerell Jr., W Im, Glycan reader: Automated sugar identification and simulation preparation for carbohydrates and glycoproteins. *J. Comput. Chem.* **32**, 3135–3141 (2011).
27. T Darden, D York, L Pedersen, Particle mesh Ewald: An N·log(N) method for Ewald sums in large systems. *The J. Chem. Phys.* **98**, 10089–10092 (1993).
28. D van der Spoel, PJ van Maaren, The origin of layer structure artifacts in simulations of liquid water. *J. Chem. Theory Comput.* **2**, 1–11 (2006).
29. B Hess, H Bekker, HJC Berendsen, JGEM Fraaije, LINCS: A linear constraint solver for molecular simulations. *J. Comput. Chem.* **18**, 1463–1472 (1997).